JOURNAL OF SYNCHROTRON RADIATION
ISSN 1600-5775

Growth of nano-dots on the grazing-incidence mirror surface under FEL irradiation

I. V. Kozhevnikov,[a]* A. V. Buzmakov,[a] F. Siewert,[b] K. Tiedtke,[c] M. Störmer,[d] L. Samoylova[e] and H. Sinn[e]

[a]Shubnikov Institute of Crystallography, Russian Academy of Sciences, Leninskiy Prospect 59, Moscow 119333, Russian Federation, [b]Helmholtz-Zentrum Berlin für Materialien und Energie GmbH, Albert Einstein Strasse 15, 12489 Berlin, Germany, [c]Deutsches Elektronen-Synchrotron DESY, Notkestrasse 85, 22603 Hamburg, Germany, [d]Helmholtz-Zentrum Geesthacht, Institute of Materials Research, Max-Planck-Strasse 1, 21502 Geesthacht, Germany, and [e]European XFEL GmbH, Albert Einstein Ring 19, 22761 Hamburg, Germany. *Correspondence e-mail: ivk@crys.ras.ru

Received 1 July 2015
Accepted 18 November 2015

Edited by M. Zangrando, Elettra and IOM-CNR, Italy

Keywords: free-electron lasers; nano-dots; FEL mirrors; interaction of FEL radiation with matter.

A new phenomenon on X-ray optics surfaces has been observed: the growth of nano-dots (40–55 nm diameter, 8–13 nm height, 9.4 dots μm^{-2} surface density) on the grazing-incidence mirror surface under irradiation by the free-electron laser (FEL) FLASH (5–45 nm wavelength, 3° grazing-incidence angle). With a model calculation it is shown that these nano-dots may occur during the growth of a contamination layer due to polymerization of incoming hydrocarbon molecules. The crucial factors responsible for the growth of nano-dots in the model are the incident peak intensity and the reflection angle of the beam. A reduction of the peak intensity (*e.g.* replacement of the FEL beam by synchrotron radiation) as well as a decrease of the incident angle by just 1° (from 3° to 2°) may result in the total disappearance of the nano-dots. The model calculations are compared with surface analysis of two FLASH mirrors.

1. Introduction

Any surface, even if placed in a vacuum, will be covered by an adhesion (contamination) layer consisting mainly of hydrocarbons and water molecules. These substances are always present even in ultrahigh vacuum, and their concentration is typically far beyond that of other materials. The contamination layer is loose, that is its density achieves a maximum value of about 1.0–1.3 g cm^{-3} near the surface and is decreasing gradually with height (Filatova *et al.*, 2012*a*,*b*; Kozhevnikov *et al.*, 2015). The adhesion film growth occurs up to a certain thickness, which does not typically exceed 1.5–2 nm, if the surface is kept in an air environment, and then the growth stops due to the concurrence between molecules adsorption and desorption processes.

The situation drastically changes if the surface is irradiated by highly intensive soft or hard X-rays, *e.g.* in the case of mirrors placed in synchrotron or free-electron laser (FEL) beamlines as well as in setups for extreme ultraviolet lithography (Boller *et al.*, 1983; Naito *et al.*, 2004; Chen *et al.*, 2009). Under the action of photoelectrons created by an incident X-ray beam at the surface (and of X-ray photons directly), large incoming hydrocarbon molecules are broken down into smaller fragments that are much more chemically active. These fragments react with each other forming strong (C—C) chemical bonds (Kurt *et al.*, 2002; Anazawa *et al.*, 2008). As a result, hydrocarbon molecules are polymerized (Anazawa *et al.*, 2008) and form a stable and rather dense film [the density achieves 1.8–1.9 g cm^{-3} (Kurt *et al.*, 2002; Anazawa *et al.*, 2008)] with the thickness increasing continuously with the

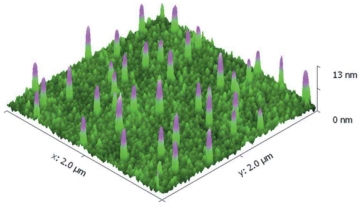

irradiation time. The carboneous contamination of the mirror surface results in a drop in reflectivity and the appearance of undesirable X-ray scattering due to the development of the surface roughness. Therefore, the mirrors have to be cleaned from time to time by, for example, RF-based plasma (Eggenstein *et al.*, 2001), atomic hydrogen (Motai *et al.*, 2008), molecular oxygen (Malinowski *et al.*, 2001) and ozone cleaning (Oestreich *et al.*, 2000) or, a more complex option, by re-polishing.

Recently a grazing-incidence plane mirror used at the BL3 beamline of the free-electron laser FLASH (Ayvazyan *et al.*, 2006; Ackermann *et al.*, 2007; Tiedtke *et al.*, 2009) at DESY (Hamburg, Germany) was the subject of investigation in order to inspect the state of its coating after three years of operation. FLASH was the first FEL providing extreme ultraviolet (XUV) and soft X-ray radiation and started user operation in 2005. It is operated in the so-called SASE (self-amplified spontaneous emission) mode in which the spontaneous undulator radiation is amplified until it saturates at a peak power of several gigawatts. Currently FLASH covers a wavelength range in the fundamental from 4.2 nm to about 45 nm with up to 3 GW peak power and pulse durations from below 50 fs to 200 fs. Short-wavelength FELs like FLASH are single-pass machines which can serve only one user at a time. In order to make efficient use of the beam time, the FLASH FEL beam can be directed to one of five experimental stations across beamlines with different characteristics, just by moving one or two plane mirrors (Tiedtke *et al.*, 2009). Due to the strong absorption of extreme ultraviolet and soft X-ray radiation in any material, particularly in air, a windowless ultrahigh-vacuum and particle-free system is used encompassing the FEL and the photon beam transport up to the experimental stations, altogether 315 m. The photon beam transport system is approximately 75 m long from the undulator exit to the endstations and includes only grazing-incidence optics.

The inspected mirror, BL3M0, was placed downstream of a first pair of mirrors serving as offset mirrors to separate potentially harmful Bremsstrahlung from the FEL radiation and was installed in a switching mirror unit to steer the beam either to the experimental station of beamline BL3 (mirror in) or to BL2 (mirror out). The distance from the undulator exit was 59.1 m. The mirror was irradiated by intensive soft X-rays with the wavelength lying in the spectral range between 5 and 45 nm. The grazing angle of the incident beam was 3°. The mirror substrate consists of single-crystal silicon. The plane mirror discussed here is of 510 mm in length, 70 mm in width and 60 mm in thickness. The aperture section is of 490 mm × 40 mm. The quality of the mirror is characterized by an overall radius of curvature of >200 km in the meridional direction, a residual slope deviation of 0.3 µrad r.m.s. as measured by use of slope-measuring deflectometry (Siewert *et al.*, 2014). The micro-roughness is 0.1 nm r.m.s. as measured by use of a white-light interferometer (WLI) (Wyant, 2002) of magnification 20× and 50×. Measurements using an atomic force microscope (AFM) were not performed before installation at the beamline. The mirror was coated with amorphous carbon

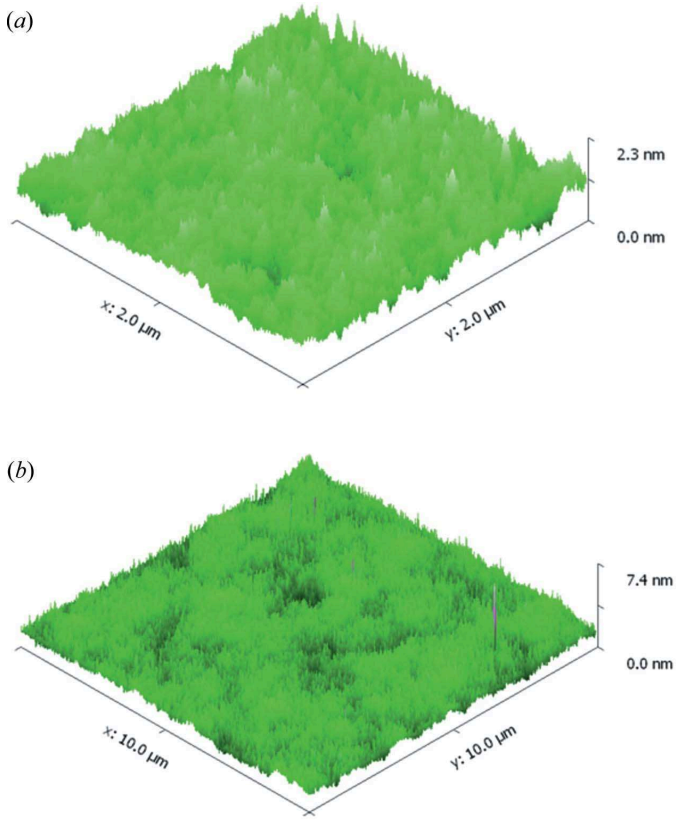

Figure 1
AFM image of the surface of mirror BL3M0 outside the irradiated area. The AFM scan was equal to (*a*) 2 µm × 2 µm and (*b*) 10 µm × 10 µm.

(a-C) of about 45 nm thickness and 2.1 g cm^{-3} density (Störmer *et al.*, 2011). The mirror surface was found to be covered by a polymerized hydrocarbon film of about 25–30 nm thickness. AFM study demonstrated that the surface roughness of the mirror was essentially increased up to 1.2 nm (10 µm × 10 µm as measured using an AFM). Fig. 1 shows the mirror BL3M0 surface *outside* the irradiated area. The surface image looks quite normal for a mirror after long-term irradiation by intensive synchrotron beam and the only feature observed in the image is essential development of the surface roughness.

A completely unexpected result is demonstrated in Fig. 2, where the mirror surface *inside* the irradiated area is shown: alot of nano-dots, which appear like spikes in the AFM images due to the strong magnification along the *Z*-direction, are placed chaotically over the mirror surface. For clarity, Fig. 3 demonstrates the surface profile along a straight line inside the irradiated area. In our opinion the growth of nano-dots has never been observed before on mirrors placed in synchrotron beamlines.

There are a number of papers [see, for example, Hau-Riege *et al.* (2007), and references therein] where damage of surfaces was observed under the action of FEL irradiation. However, these experiments were performed at normal or near normal incidence of the FEL beam focused into a spot of size a fraction of a micrometer, so that the surface damage was often observed under the action of a single pulse only and was

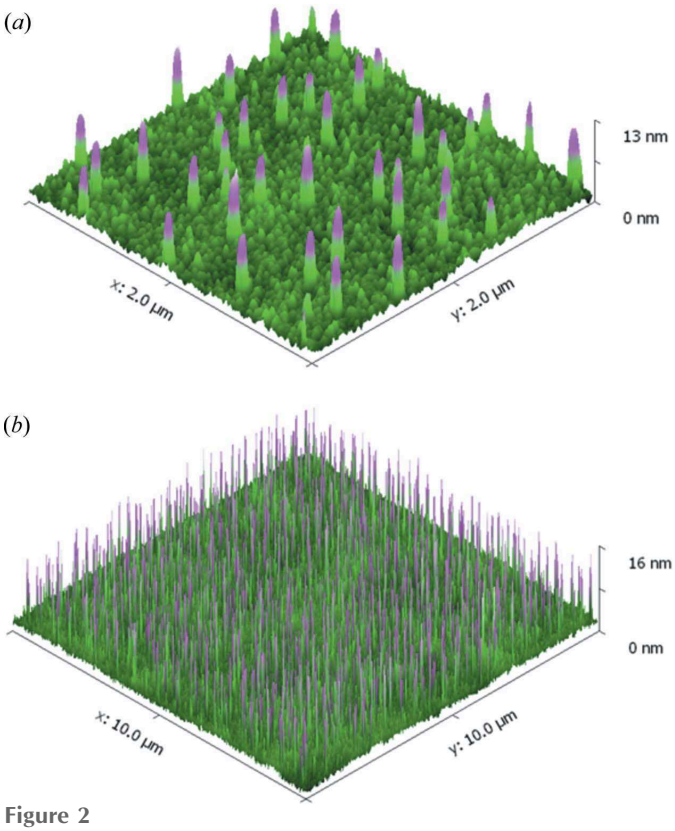

Figure 2
AFM image of the surface of mirror BL3M0 inside the irradiated area. The AFM scan was equal to (*a*) 2 µm × 2 µm and (*b*) 10 µm × 10 µm.

caused by, for example, ablation of material. Re-deposition of the ablated material results often in the appearance of spikes situated near the crater. Modeling given by Hau-Riege *et al.* (2007) was based on the approach developed initially for analysis of the dynamics of hot-dense plasma.

In our case the mirror was irradiated at very small grazing angles, the beam footprint was tens of centimeters, the effect was observed after several years of mirror operation at the beamlines, and craters caused by ablation of material were not detected on the surface. Note that mirrors at the FLASH beamlines remain 'cold' under irradiation and do not demand additional cooling. Therefore, we believe that we observed a new physical phenomenon, which has not been discussed before in the literature.

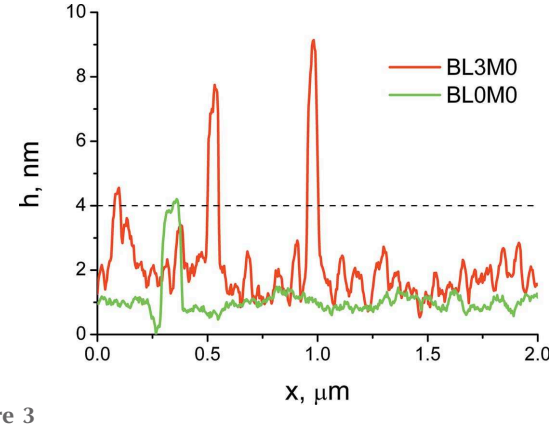

Figure 3
Surface profiles along a line inside the irradiated area of mirrors BL3M0 and BL0M0. The zero level corresponds to the deepest minimum on the surface. Spikes on mirror BL3M0 are supposed for definiteness to be the surface features whose height exceeds 4 nm.

In parallel to BL3M0, one further mirror, BL0M0, was inspected. BL0M0 was the first mirror in the photon beam distribution system and was placed 48 m distance from the undulator exit. The mirror was fabricated by the same producer as BL3M0, has the same geometrical parameters as BL3M0, the same carbon coating, the same roughness before installation at the beamline, and was operated for about the same time under conditions similar to BL3M0 except for one distinction, namely, a slightly different grazing angle of the incident FEL beam: 3° for BL3M0 compared with 2° for BL0M0.

An AFM image of the mirror BL0M0 surface *inside* the irradiated area is shown in Fig. 4. In contrast to Fig. 2, there are no clearly observed nano-dots, while a number of spikes of several nanometers in height are distinguishable. The surface profile along a straight line is shown in Fig. 3, the line having passed through the highest spike observed on the AFM image. Comparing Fig. 2 and Fig. 4 we can conclude that the growth of nano-dots is essentially suppressed on the mirror BL0M0 surface.

Therefore, three fundamental questions arise:

(i) What is the physical reason for the nano-dots growth under FEL irradiation?

(ii) Why have such nano-dots not been observed on mirrors in synchrotron beamlines at third-generation storage rings?

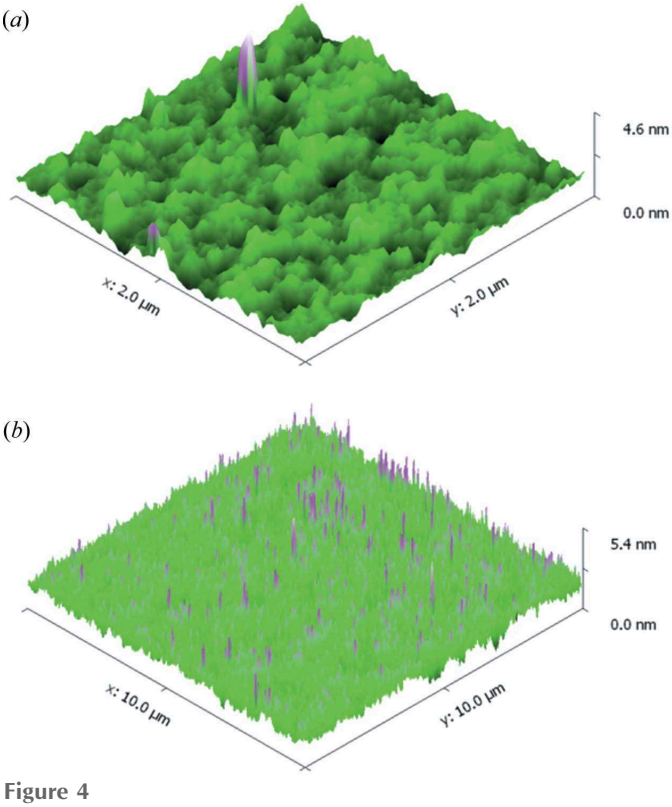

Figure 4
AFM image of the surface of mirror BL0M0 inside the irradiated area. The AFM scan was equal to (*a*) 2 µm × 2 µm and (*b*) 10 µm × 10 µm.

(iii) Why have the spikes appeared on mirror BL3M0 placed under a 3° grazing angle with respect to the FEL beam but are poorly distinguishable on mirror BL0M0 placed under 2° grazing angle?

The answers to these questions are the goal of the present paper.

Below we will demonstrate that the phenomenon of hydrocarbon molecules polymerization may explain the appearance and growth of nano-dots on the mirror surface, if we take into account the high intensity of the FEL beam, random fluctuations of the incoming flux of hydrocarbon molecules and the roughness of the virgin reflective surface.

The main idea of our approach is based on the assumption that the growth of nano-dots is caused by polymerization (cracking and subsequent strong chemical bonding) of incoming hydrocarbon molecules. The probability of polymerization is proportional to the density of photoelectrons at the point of the molecule dropping onto the surface, which, in turn, is proportional to the radiation power absorbed in the matter, *i.e.* the value of the field intensity (the radiation flux density) $|E|^2$. The variation of the field intensity near an ideally smooth flat surface (plane $z = 0$) is shown in Fig. 5, curve 1. The z-axis is directed into the substrate. The grazing angle of the incidence beam (wavelength $\lambda = 10$ nm) is small ($\theta = 3°$) so that the field intensity on the surface is low, while it is increased in a vacuum with increasing distance from the surface. Therefore, if there is a feature (a peak) on the surface, the field intensity on the feature's top is higher (by about a factor of five in Fig. 5) and, hence, the probability of polymerization of incoming molecules increases resulting in a quicker growth of the feature as compared with the growth of the underlying surface. Therefore, positive feedback arises: the higher the feature on the surface, the quicker its growth occurs and finally the feature appears as a spike or nano-dot.

In the following section we describe briefly the statistical parameters of the nano-dots observed in our experiment. The growth model, which we use for analysis of the nano-dots

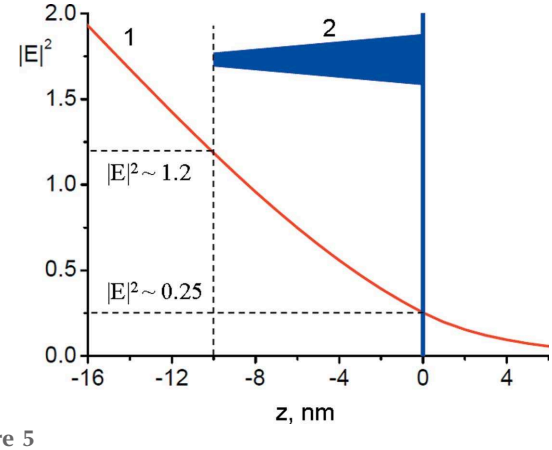

Figure 5
Sketch explaining the main idea of our approach: the higher the feature (2) on the surface, the quicker its growth occurs due to polymerization of incoming molecules. The distribution of the field intensity (1) near the carbon surface was calculated assuming an incidence of soft X-rays of 10 nm wavelength at 3° grazing angle. The z-axis is directed into the substrate.

growth, is explained in detail in §3. The growth of the polymerized film on the ideally smooth surface is analyzed in §4. We demonstrate that even in this case the nano-dots can occur, due to stochastic fluctuations of the incident molecule flux resulting in the appearance of inhomogeneities (roughness) on the growing surface and, thus, the appearance of positive feedback as mentioned above. The growth of nano-dots is demonstrated to occur only if the field intensity is high enough. The growth of the polymerized layer on a rough surface is considered in §5. In this case the nano-dots are demonstrated to grow at once on the substrate areas placed above the averaged surface plane as the positive feedback in the polymerization process appears from the beginning of the contamination layer formation. The dependence of the nano-dots growth on the grazing angle of incident radiation is analyzed in §6. We demonstrate that the growth of nano-dots is clearly observed in a limited, from above and below, interval of the grazing-incidence angle. Decreasing the angle from 3° to 2° is shown to result in the almost total disappearance of the nano-dots on a mirror surface for the same incoming beam parameters. The main results of the paper are summarized in §7.

2. Nano-dots statistic

In this section we briefly analyze the statistical parameters of nano-dots (spikes) observed on the AFM images of the mirror surface inside the irradiated area (Fig. 2). The instrument used is a Bruker SIS-Ultraobjective AFM with a 40 µm × 40 µm scanner. The tip applied for these measurements is a silicon SPM-sensor for the non-contact mode, with resonance frequency 190 kHz and force constant 48 N m^{-1}. The tip is shaped like a polygon-based pyramid with a height of 10–15 µm. The tip radius is less than 8 nm.

By convention we will consider the spikes as peaks on the surface, whose height exceeds $h = 4$ nm, where the zero level $h = 0$ corresponds to the deepest minimum on the surface image. In other words, spikes are the features placed above the straight dashed line in Fig. 3. Then we can divide the irradiated surface (Fig. 6*a*) on the underlying surface with cutting spikes (Fig. 6*b*) and spikes or nano-dots (Fig. 6*c*). The surface density of the dots proved to be about 9.4 dots µm^{-2}.

First of all, we found that all three objects considered (the irradiated surface, the underlying surface and the nano-dots) are uniform and isotropic in the XY plane. The latter conclusion was checked by analysis of the two-dimensional PSD function,

$$\mathrm{PSD}_{2\mathrm{D}}(f_x, f_y) = \frac{1}{L^2}\left\{\sum_{n,m=1}^{N} h(x_n, y_m) \times \exp\left[2i\pi\Delta L\left(n f_x + m f_y\right)\right](\Delta L)^2\right\}^2,$$

in the plane of the spatial frequencies (f_x, f_y). The PSD function of the three objects studied was found to be circular

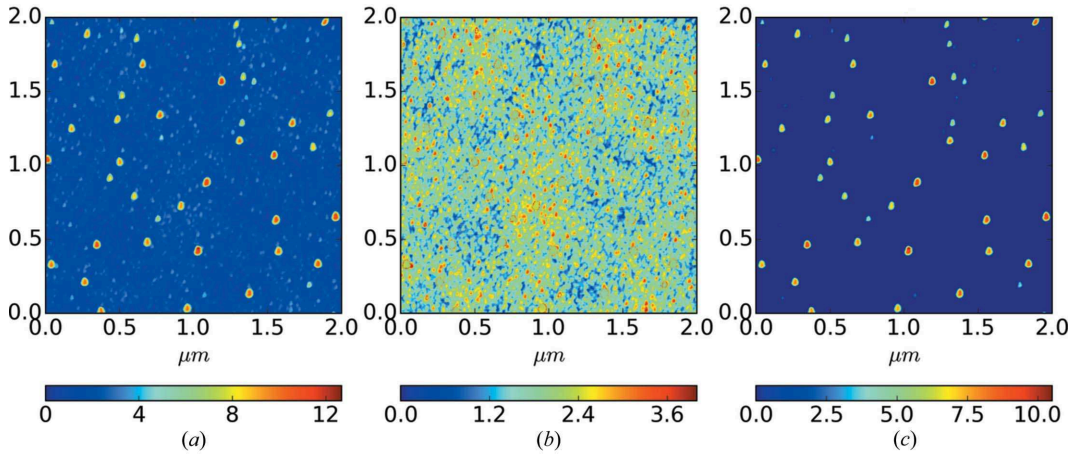

Figure 6
AFM image of the irradiated surface of mirror BL3M0 (*a*), the underlying surface (*b*) and the nano-dots (*c*). The AFM scan was 2 μm × 2 μm.

symmetrical, *i.e.* it depends only on the modulus of the spatial frequency $f = (f_x^2 + f_y^2)^{1/2}$ demonstrating isotropy.

The PSD functions deduced from the AFM measurements are presented in Fig. 7 (red curves), for the virgin surface (*a*), the underlying surface (*b*) and the nano-dots (*c*). The root-mean-squared (r.m.s.) roughness $\sigma = [\int \mathrm{PSD}_{2\mathrm{D}}(f)\, f\, \mathrm{d}f]^{1/2}$ in the measured interval of the spatial frequency is equal to 1.2 nm for the virgin surface, 0.6 nm for the underlying surface and 1.0 nm for the dots.

As the intensity of radiation scattered by the surface roughness (including nano-dots) is proportional to the PSD function, the growth of the nano-dots results in an essential increase in the scattered intensity, thus spoiling the beam performance.

The distributions of the nano-dot heights, the nano-dot diameters in the bottom section (at $h = 4$ nm in Fig. 3) and the distances between two closest dots are shown in Fig. 8. The spike heights in Fig. 8(*a*) were measured from the averaged underlying surface $h = \bar{h}$ as in Fig. 6(*b*). Here ΔM is the number of nano-dots in an individual column, and $M = 937$ is the total number of dots in the 10 μm × 10 μm AFM image. The mean values of these parameters are $\langle h \rangle \simeq 9.9$ nm, $\langle d \rangle \simeq 46$ nm and $\langle l \rangle \simeq 223$ nm. The total area of the nano-dot sections (at $h = 4$ nm in Fig. 3) is 1.6 μm^2, *i.e.* 1.6% of the surface area. The maximum observed in the PSD function of the nano-dots (Fig. 7*c*) corresponds to the peak in the distribution of the distances between neighboring dots (Fig. 8*c*).

We attempted to perform a similar analysis for mirror BL0M0. However, we found that there is a problem distinguishing between nano-dots and 'conventional roughness'. Actually, there is only one spike exceeding 4 nm, the value being measured from the deepest minimum on the surface image, and shown in Fig. 3. The rest of the peaks are essentially lower; the number of peaks higher than 3 nm being only 23 and higher than 2 nm being 356. The distribution of the surface peak heights measured from the averaged underlying surface is shown in Fig. 8(*a*). In contrast to mirror BL3M0, the distribution function decreases monotonically with increasing height without clearly pronounced peaks caused by nano-dots.

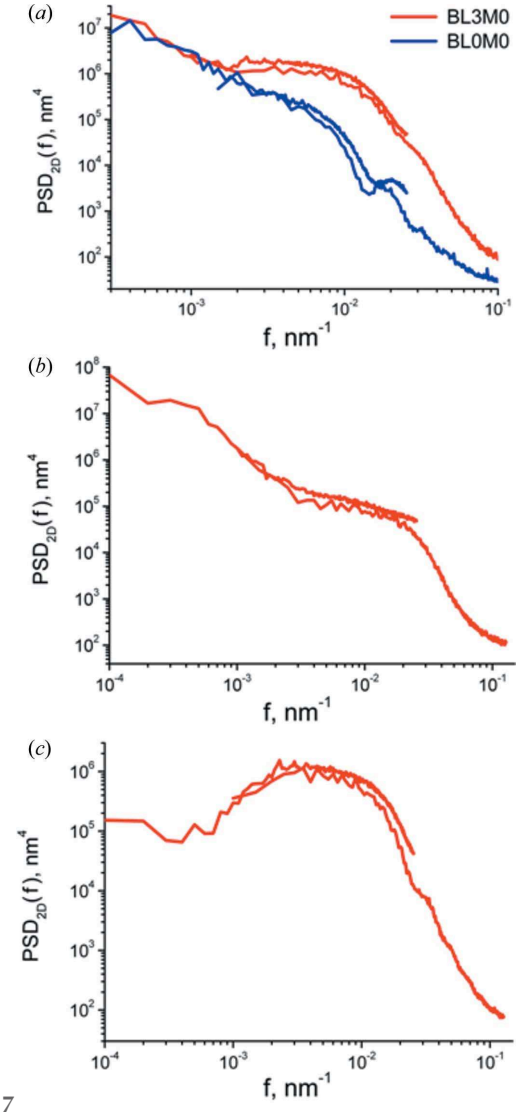

Figure 7
Two-dimensional PSD function of the irradiated surface of mirror BL3M0 (red curves) (*a*), the underlying surface (*b*) and the nano-dots (*c*). The functions were deduced from AFM scans of 10 μm × 10 μm and 2 μm × 2 μm and were smoothed over statistical oscillations for clarity. The PSD function of the irradiated surface of mirror BL0M0 (blue curves) is also shown for comparison.

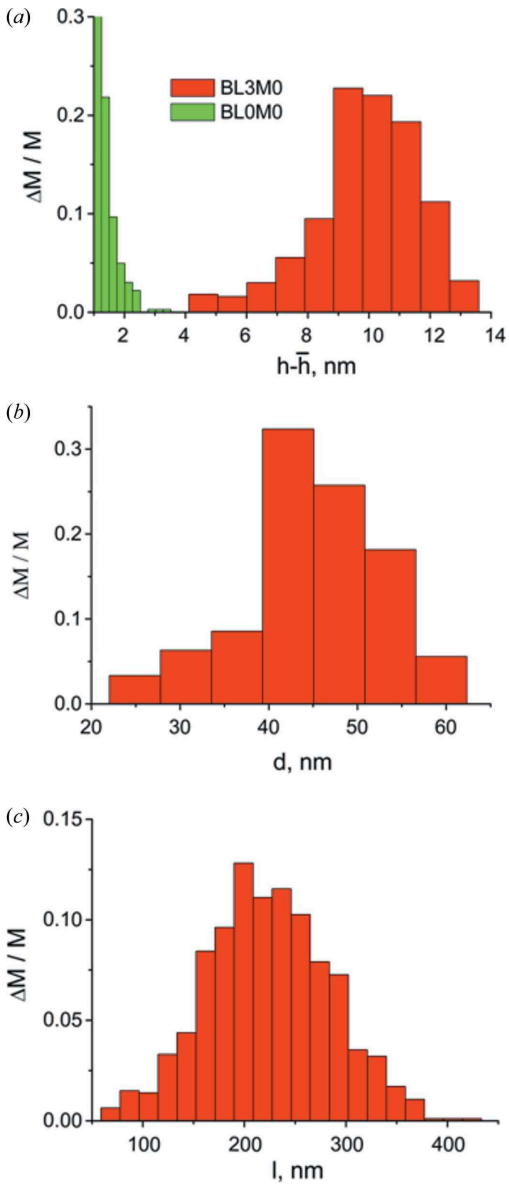

Figure 8
Distributions of the nano-dots height h on mirror BL3M0 (a), the nano-dots diameter d in the bottom section (b), and the distance l between two closest dots (c). The distributions of the nano-dots height h on mirror BL0M0 is also shown in (a) for comparison. The spike heights were measured from the averaged underlying surface.

Therefore the other statistical distributions are not shown in Figs. 8(b) and 8(c) because of the too low number of nano-dots that can be trustworthy recognized on the mirror BL0M0 surface.

The two-dimensional PSD function of the mirror BL0M0 surface is shown in Fig. 7(a) (blue curves). In contrast to the BL3M0 mirror, where the well pronounced 'hump' caused by nano-dots is seen, the PSD function of mirror BL0M0 decreases gradually with spatial frequency and demonstrates behavior that is quite typical for the external film surface roughness (see, for example, Peverini *et al.*, 2007; Filatova *et al.*, 2010). The r.m.s. roughness of mirror BL0M0 is equal to about 0.35 nm in the measured interval of the spatial frequency, *i.e.* almost two times less as compared with the underlying surface (nano-dots excluded) of mirror BL3M0.

Thus, based on the AFM image and the statistical analysis of the surface roughness we can conclude that the earliest stage of nano-dots growth is observed on the mirror BL0M0 surface.

3. Growth model

For simplification we consider a 1+1-dimension model of the polymerized film growth and assume that the process is continuous in time, while in reality irradiation of the mirror surface occurs at the expense of short FEL impulses. We analyze the process using the vivid approach of Family and Viscek (Family & Vicsek, 1985; Family, 1986), where the film growth is modeled by representating the incoming molecules flux as a set of small cubes of size a falling vertically onto the surface of length $L = aM$ (M is an integer) and forming growing columns of height h_j ($j = 1, \ldots, M$ is the number of columns). The process is schematically shown in Fig. 9.

We assume that three, and only three, different events may occur after a molecule falls onto the surface. First, the molecule dropped in column j sticks at once to its top due to polymerization under the action of photoelectrons. Let $P_{\rm pol}$ be the probability of this event. Second, the molecule may be reflected (desorbed) from the surface with the probability $P_{\rm des}$. Thirdly, the molecule may diffuse along the surface with the probability $P_{\rm dif} = 1 - P_{\rm pol} - P_{\rm des}$, whereupon it sticks to the surface due to polymerization. The experimental values of the probabilities $P_{\rm des}$ and $P_{\rm dif}$ are scarcely known, and their calculation from first principles is a very complex problem, if at all possible. Therefore the ratio $P_{\rm des}/P_{\rm dif}$ is considered below as the free parameter of our qualitative modeling.

The probability of polymerization $P_{\rm pol}$ is supposed to be proportional to the photoelectron density $Q(x, h)$ at the point of the molecule drop onto surface. In turn, the density Q is proportional to X-ray radiation absorption in the matter, *i.e.* $Q(x, h) \simeq |E(x, h)|^2 \,{\rm Im}\,\varepsilon$, where ε is the complex dielectric constant of the matter and E is the field function written in the first approximation as

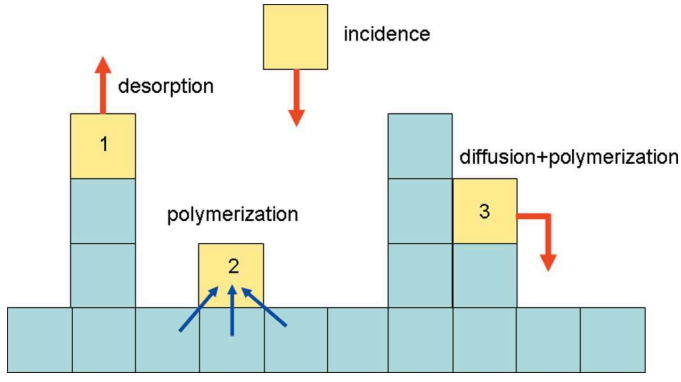

Figure 9
Schematic of the adhesion layer growth.

$$E(x, h) = A\exp(ik_x x)E_0(h - \bar{h}),$$

$$E_0(h - \bar{h}) = \begin{cases} \exp[-ik_z(h - \bar{h})] + r(\theta)\exp[ik_z(h - \bar{h})], & \text{if } h - \bar{h} > 0 \\ t(\theta)\exp[-i\kappa_z(h - \bar{h})\sin\theta], & \text{if } h - \bar{h} < 0, \end{cases}$$

$$k = 2\pi/\lambda, \quad k_x = k\cos\theta,$$

$$k_z = k\sin\theta, \quad \kappa_z = k\left(\varepsilon - \cos^2\theta\right)^{1/2},$$

$$r(\theta) = (k_z - \kappa_z)/(k_z + \kappa_z), \qquad t(\theta) = 2k_z/(k_z + \kappa_z), \tag{1}$$

where A is the field amplitude, θ is the grazing angle of the incident wave, λ is the wavelength, $r(\theta)$ and $t(\theta)$ are the amplitude reflectance and transmittance determined by the Fresnel formulas, respectively, and $\bar{h} = \sum_{j=1}^{M} h_j/M$ is the average thickness of the adhesion film.

The grazing angle of the incident beam θ and the radiation wavelength λ are set below to $\theta = 3^\circ$ and $\lambda = 10$ nm. For the chosen values of λ and θ the reflectivity $R = |r|^2 \simeq 93.35\%$ and the field intensity on a perfectly smooth carbon-coated surface $|E_0(0)|^2 = |t(\theta)|^2 \simeq 0.253$. The representation (1) for the field near a rough surface is valid if the r.m.s. roughness σ is small enough, namely, $\sigma < \lambda/(4\pi\sin\theta) \simeq 15$ nm.

The effect of the substrate is neglected in (1) or, equivalently, the substrate material is supposed to be the same as that of the adhesion film. The fact is that we will consider only the incidence of soft X-ray radiation at very small grazing angle, when the effect of the substrate on the wavefield is negligible beginning from a film thickness of about 5 nm. Moreover, the studied mirror was covered from the outset by the carbon reflective coating of density close to that of the polymerized layer.

The probability of polymerization of a molecule dropped on a surface depends on the environment of the molecule. We would expect that the photoelectron density and, hence, the probability of polymerization is lower for molecule 1 in Fig. 9 compared with those for molecules 2 and 3. For simplicity we will suppose that the photoelectron density at the point of the molecule drop is proportional to the number of molecules $N_{\rm eff}$ touching the molecule under consideration. In particular, the value of $N_{\rm eff}$ is equal to 1, 3 and 4 for molecules 1, 2 and 3 in Fig. 9, respectively. In general, we can introduce the contribution weight of the surrounding molecules to the photoelectron density at the point considered. As an example, we calculated the adhesion layer growth assuming the neighbor molecule contributes to the value of $N_{\rm eff}$ by the weight of unity or a half depending on whether it touches the considered molecule by face or by edge, respectively. However, the growth regularities remained the same qualitatively.

Thus, we can represent the probability of polymerization of the molecule dropped onto the top of the jth column as $P_{\rm pol}(h_j) = \eta_0 N_{\rm eff}|E_0(h_j - \bar{h})|^2$, where the free parameter of the model η_0 is proportional to the field amplitude A^2. In other words, increasing the parameter η_0 by n times corresponds to an increase in the incident wave intensity (radiation flux density) by the same factor. To guarantee the polymerization probability to be always less than unity, we re-write the expression for $P_{\rm pol}$ as follows,

$$P_{\rm pol}(h_j) = 1 - \exp\left[-\eta_0 N_{\rm eff}\left|E_0(h_j - \bar{h})\right|^2\right]. \tag{2}$$

For illustrative purposes, we will use below the value of the polymerization probability P_0 of the molecule falling onto the flat surface when $N_{\rm eff} = 3$ and $h_j = \bar{h}$,

$$P_0 = 1 - \exp\left[-3\eta_0\left|t(\theta)\right|^2\right]. \tag{3}$$

Modeling of the adhesion layer growth consists of the following. At first we generate the random number j from a set of integer numbers $\{j\}$ distributed uniformly in the interval $[1, M]$. The number corresponds to the number of the column which the molecule drops on. Then we calculate the field on top of the column using (1), determine the number of surrounding molecules $N_{\rm eff}$ and find the probability of polymerization $P_{\rm pol}$ *via* (2). After that we generate the random number p from a set of real numbers $\{p\}$ distributed uniformly in the interval $[0, 1]$ and choose one of three possible events, namely polymerization, desorption or diffusion of the molecule depending on the subinterval $[0, P_{\rm pol}]$, $[P_{\rm pol}, P_{\rm pol} + P_{\rm des}]$ or $[P_{\rm pol} + P_{\rm des}, 1]$, respectively, where the generated number p lies. If polymerization of the molecule occurs, the height of the jth column is increased by a. In the case of desorption, the molecule disappears and the surface relief is not changed. In the case of diffusion and following Family (1986), we consider the nearest-neighbor diffusion only, *i.e.* the molecule dropped in column j sticks to the top of column $j - 1$, j or $j + 1$, depending on which of these columns has the smallest height. If columns $j - 1$ and $j + 1$ are of the same height, and both of them are lower than column j, we generate an additional random number distributed uniformly in the $[0, 1]$ interval. The direction of the molecule diffusion (to the right or left) is chosen according to whether the generated number is more or less than 0.5 and the height of column $j + 1$ or $j - 1$ is increased by a. The process of the molecule drop is repeated time and again until the necessary average thickness of the adhesion layer is achieved. Note again that the free parameters of the modeling are η_0 in (2), the ratio $P_{\rm des}/P_{\rm dif}$ and the molecule size a.

4. Growth of nano-dots on a perfectly smooth substrate

First of all we consider growth of an adhesion layer on an ideally smooth substrate and demonstrate that the nano-dots can arise from the noise (random fluctuations) of the incident molecules flux under a special choice of the free parameters η_0 and $P_{\rm des}/P_{\rm dif}$ of the growth model.

An example is presented in Fig. 10. For definiteness we assumed that the size of hydrocarbon molecules is equal to $a = 0.25$ nm and the probability of desorption is equal to that of diffusion, *i.e.* the ratio $P_{\rm des}/P_{\rm dif} = 1$. Fig. 10(*a*) demonstrates the growth of the adhesion film at the value of the parameter $\eta_0 = 0.03$, which corresponds to the probability (3) of the molecule polymerization at the flat surface $P_0 = 2.2\%$. The

profiles shown in the figure were calculated after equal temporal intervals corresponding to a drop onto a surface of 5×10^5 molecules, while part of them were desorbed. As may be seen, the profiles are rather smooth, because of the strong effect of surface diffusion. Evidently, a decrease in the parameter η_0, *i.e.* in the incident radiation intensity, keeps the growth pattern practically the same.

However, if the radiation intensity is enhanced by a factor of five, the parameter η_0 increased up to 0.15 and the probability of polymerization on the flat surface up to 10.7%, the growth regularities are drastically changed (Fig. 10*b*). Starting from a layer thickness of about 100 nm, the swift growth of spikes is clearly observed. Notice that the same sets of random numbers were used when calculating Figs. 10(*a*) and 10(*b*). In addition, we calculated the layer growth using several other sets of random numbers, while the growth pattern proved to be very similar qualitatively with those shown in Fig. 10. Therefore, the difference between the two growth patterns observed in Figs. 10(*a*) and 10(*b*) is connected to the physical mechanism of growth (positive feedback in polymerization with the nano-dots growth) rather than to accidental difference in the molecule fluxes. Comparison of Figs. 10(*a*) and 10(*b*) demonstrates clearly that the crucial factor providing the dots growth is high radiation intensity. Increasing the radiation flux density by several times only (*e.g.* replacement of synchrotron beam by FEL radiation) may result in a radically new pattern of adhesion film growth.

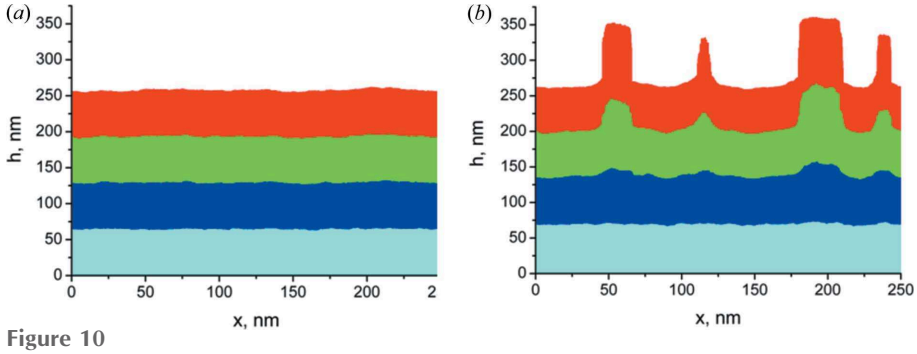

Figure 10
Growth of the contamination film on an initially flat surface at different values of parameter η_0, *i.e.* 0.03 (*a*) and 0.15 (*b*), resulting in the probability of polymerization at a flat substrate $P_0 = 2.2\%$ (*a*) and 10.7% (*b*). The ratio $P_{des}/P_{dif} = 1$ is the same in both cases. The cube size is $a = 0.25$ nm. The same sets of random numbers $\{j\}$ and $\{p\}$ were used when modeling the growth of the films.

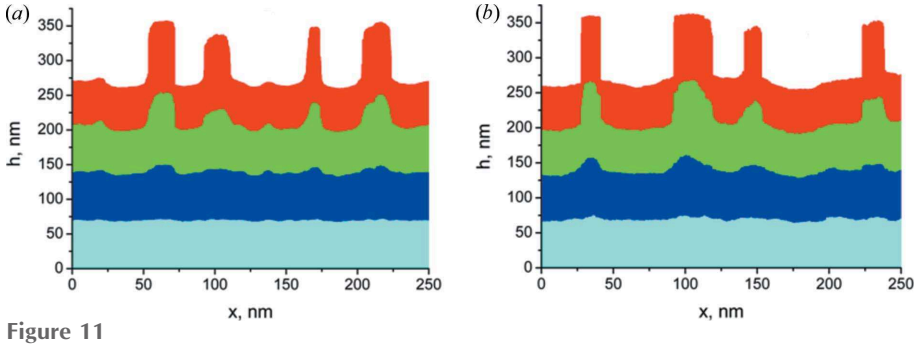

Figure 11
The same as in Fig. 10(*b*), but for a cube size of $a = 0.125$ nm (*a*) and 0.5 nm (*b*).

Notice that the necessary condition ($\sigma < 15$ nm) of the validity of (1) used under modeling the adhesion layer growth is not obeyed for the red profile in Fig. 10(*b*) (the thickest film), which, thus, can be only considered as a qualitative result.

Let us analyze now the effect of the free parameters on the regularities of the nano-dots growth. The growth of the adhesion layer is shown in Fig. 11 for the same parameters as for Fig. 10(*b*) ($\eta_0 = 0.15$ and $P_{des}/P_{dif} = 1$) except for the cube size a, which is equal to 0.125 nm (Fig. 11*a*) or 0.5 nm (Fig. 11*b*). These values seem to be the minimal and maximal possible size of hydrocarbon molecules, respectively. While some difference in statistical parameters of the profiles is observed in Figs. 10(*b*), 11(*a*) and 11(*b*), the patterns of the growth are qualitatively the same in all three graphs. Therefore, below we will set the molecule size $a = 0.25$ nm for definiteness.

The effect of the parameter P_{des}/P_{dif} on the nano-dots growth is far beyond that of the molecule size. An example is presented in Fig. 12, where several profiles of the adhesion layer surface are shown after falling onto the surface of 2×10^6 molecules. The layer growth was modeled at a different probabilities ratio P_{des}/P_{dif} varying from zero (curve 1) to infinity (curve 5). The parameter η_0 was set to 0.1 so that the probability of polymerization on the flat surface is $P_0 = 7.3\%$. The same sets of random numbers were used for modeling the growth of all films. The rather different average thickness of the adhesion layer is explained by the different probability of desorption. In particular, the probability of desorption is equal to zero for profile 1, *i.e.* all molecules dropped onto the surface

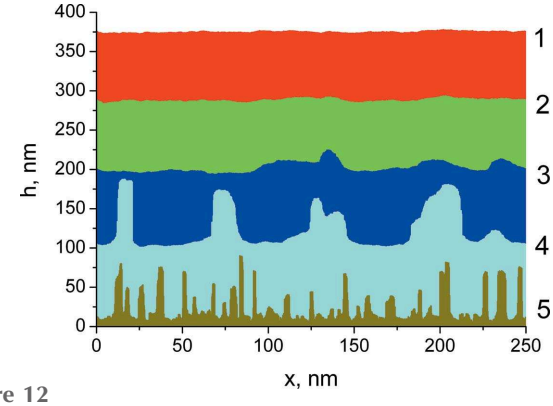

Figure 12
Growth of the adhesion film on an initially smooth surface at different ratios $P_{des}/P_{dif} = 0/1$ (1), 1/3 (2), 1/1 (3), 3/1 (4) and 1/0 (5). Parameter $\eta_0 = 0.1$ so that $P_0 = 7.3\%$ in all cases. The cube size is $a = 0.25$ nm. When modeling the growth of different films the same sets of random numbers $\{j\}$ and $\{p\}$ were used.

stick to it. On the contrary, the probability of diffusion is equal to zero for profile 5, so that molecules are either polymerized at the moment of dropping or desorbed from the surface, and the probability of desorption is extremely high as the parameter η_0 (and hence P_0) is rather small in the example considered.

Fig. 12 demonstrates clearly that the larger the effect of diffusion resulting in a smoothening layer surface, the later the growth of the spikes starts, if at all. Notice that the non-zero probability of desorption is a crucial factor in our modeling. Actually, the nano-dots can grow only if the combined molecule flux on its top, *i.e.* the difference between the incident and reflected molecule fluxes, exceeds that on the underlying surface. As the incident flux is the same, such a situation takes place only if the probability of desorption is non-zero, and it is decreased with the spike height.

Therefore, we demonstrated that the nano-dots may arise even on a perfectly smooth substrate, if (*a*) the radiation flux density is high enough, (*b*) the probability of desorption is non-zero, and (*c*) the probability of the surface diffusion is not very high. The cause of the nano-dots occurrence is stochastic fluctuations of the incoming molecule flux. However, Figs. 10–12 demonstrate that the dots appear at rather large thickness of the polymerized film (except the non-physical case of the absence of surface diffusion), the dots' width is very small (from several to 20–30 nm), and the distance between neighboring dots is also small (from several to 50–60 nm as a rule). These values are in rather poor agreement with those observed experimentally and described in §2.

5. Growth of a polymerized contamination layer on a rough substrate

Evidently, no real surface can be considered as perfectly smooth for soft X-rays. The surface roughness results in inequality of different parts of the substrate surface from the point of view of the adhesion layer growth. There are areas placed above the averaged surface plane where, thus, the field intensity and the probability of polymerization [equation (2)] exceed the mean values. Hence, there are a set of areas where the nano-dots can start to grow from the substrate surface at once, because the positive feedback in the polymerization process appears from the beginning of the adhesion layer formation, stochastic fluctuations of the hydrocarbon molecule flux playing an insignificant role.

Let us consider the example presented in Fig. 13 where a parabolic-shaped feature is placed on a virgin substrate, the feature width and maximal height being 80 nm and 1.5 nm, respectively (profile 1). Profiles 2, 3 and 4 show the adhesion layer relief after falling of 1×10^5 molecules, the ratio $P_{\rm des}/P_{\rm dif}$ being equal to 1/3 (profile 2), 1 (profile 3) and 3 (profile 4). Parameter η_0 was set to 0.25 so that the polymerization probability on the flat surface was $P_0 = 17.3\%$. As can be seen, in the case when the surface diffusion is rather weak (profile 4, $P_{\rm des}/P_{\rm dif}$ = 3/1), the well pronounced spike is aroused, while the averaged adhesion layer thickness is only 28.6 nm (averaging was performed over an area out of the surface feature).

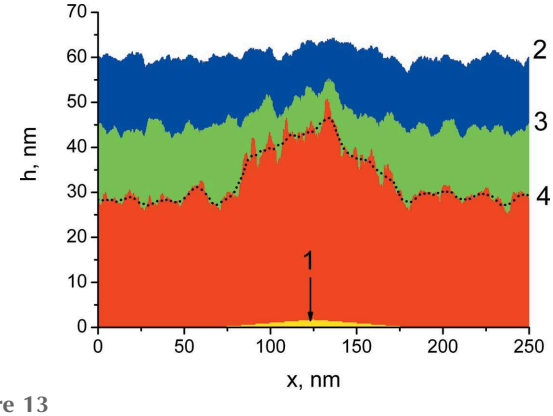

Figure 13
Surface profile of the adhesion film on a substrate with a parabolic-shaped feature (1). The width of the feature was 80 nm, and its maximal height was 1.5 nm. Modeling was performed for different ratios $P_{\rm des}/P_{\rm dif}$ = 1/3 (2), 1/1 (3) and 3/1 (4). Parameter $\eta_0 = 0.25$ so that $P_0 = 17.3\%$. The cube size was $a = 0.25$ nm. The grazing angle of the incident beam was 3°. When calculating different films, the same sets of random numbers $\{j\}$ and $\{p\}$ were used. The dotted curve shows profile 4 after averaging over 10 nm intervals along the *X*-axis.

The height of the spike counted from the averaged surface is of the order of 15 nm, while the height of the feature on the virgin surface was only 1.5 nm. The spike width (∼80 nm) corresponds to that of the virgin surface feature. Finally, the dotted curve in Fig. 13 shows profile 4 averaged over 10 nm intervals along the *X*-axis, whose value corresponds to the spatial resolution in our AFM measurements.

When the diffusion process, *i.e.* the surface smoothening, becomes more and more significant (profiles 3 and 2), the nano-dot decreases and then disappears, while the averaged thickness of the adhesion layer increases.

Evidently, the higher the virgin substrate feature, the quicker the spike growth. An example is given in Fig. 14, where profiles of the adhesion layer (averaged over 10 nm interval along the *X*-axis) are shown for different heights of the feature on the virgin substrate from 0.5 nm (curve 1) up to

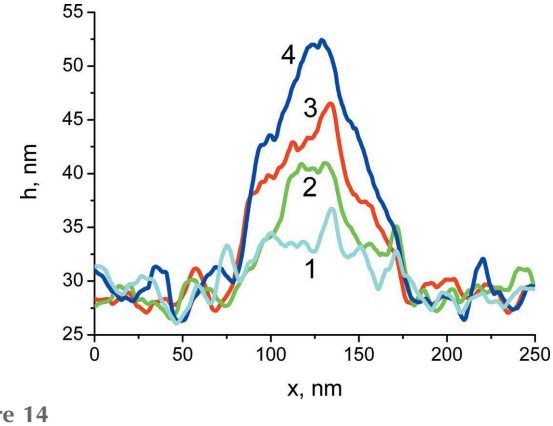

Figure 14
Profile of the adhesion layer grown on the substrate with the parabolic feature on its surface. The maximal height of the feature was 0.5 nm (1), 1 nm (2), 1.5 nm (3) and 2.5 nm (4), while the 80 nm feature length was fixed. The profiles were averaged over 10 nm intervals along the *X*-axis. The growth parameters are: $P_{\rm des}/P_{\rm dif} = 3$, $\eta_0 = 0.25$, $a = 0.25$ nm and $\theta = 3°$. The same sets of random numbers $\{j\}$ and $\{p\}$ were used when calculating different adhesion films.

2.5 nm (curve 4). The growth parameters correspond to those for profile 4 in Fig. 13: $P_{des}/P_{dif} = 3$, $\eta_0 = 0.25$ and $\theta = 3^\circ$. In the example considered the spike height with respect to the averaged surface is approximately ten times larger than that of the virgin substrate feature, *i.e.* the speed of the spike growth is approximately proportional to the feature height.

Let us consider now the growth of an adhesion layer on a rough surface. To generate the rough substrate profile we use the method described by Asadchikov *et al.* (2004). For definiteness we assume that the roughness heights are distributed according to the normal law, and the correlation function of the roughness has the following form,

$$C(x) = \sigma^2 \exp\left[-(x/\xi)^{2\alpha}\right], \qquad (4)$$

where σ is the r.m.s. roughness, ξ is the correlation length and α is the parameter connected with the fractal dimensionality D of a surface as $D = 2 - \alpha$ (Barabási & Stanley, 1995).

Three model substrate surfaces are shown in Fig. 15. The roughness parameters were chosen in (4) as $\sigma = 0.5$ nm, $\alpha = 0.8$ [profile (*a*)], $\sigma = 0.25$ nm, $\alpha = 0.8$ [profile (*b*)] and $\sigma = 0.5$ nm, $\alpha = 0.2$ [profile (*c*)]. The correlation length $\xi = 100$ nm was the same for all profiles. The number of points on the digitized profiles was 4000, which corresponds to the cube size $a = 0.25$ nm when modeling the adhesion layer growth. We used the same set of random numbers when generating the surface profiles. Therefore, the profiles (*a*) and (*b*) are very similar to each other as they differ by the r.m.s. roughness only. Moreover, the profile (*c*), being averaged over the *x*-axis, is also similar to the profile (*a*).

The growth of the adhesion layer on rough substrates is demonstrated in Fig. 16. The graphs labeled (*a*), (*b*) and (*c*) correspond to the substrate (*a*), (*b*) and (*c*) shown in Fig. 15. The total number of molecules dropped on the surface was 1.2×10^6. Profiles 1, 2 and 3 were calculated for different ratios $P_{des}/P_{dif} = 1$, 3 and 9, respectively. The polymerization parameter η_0 was set to 0.25. In addition, Fig. 16(*d*) shows the growth of the contamination layer on the substrate (*a*) [as in Fig. 16(*a*)], but for five times lower radiation intensity, *i.e.* for the parameter $\eta_0 = 0.05$.

The figure demonstrates all features of spikes growth discussed above. First, the growth speed increases with increasing height of the surface roughness [compare Figs. 16(*a*) and 16(*b*)]. Second, the spikes are clearly observed if the surface diffusion is rather weak (profiles 2 and 3 in the figure), while increasing the diffusion effect results in essentially smoothening of the spikes (profiles 1). Third, the adhesion layer profile correlates with that of the substrate if the diffusion effect is weak (profiles 2 and 3). Fourth, decreasing radiation intensity results in disappearance of the spikes [compare Figs. 16(*a*) and 16(*d*)]. In addition, Fig. 16 shows that statistical parameters of the spikes depend heavily on the fractal parameter α of the virgin surface.

Let us consider profiles 3 in Figs. 16(*a*) and 16(*c*). As in §2, we analyze only surface features whose height exceeds, say, 20 nm, *i.e.* the features placed above the dashed straight lines in Figs. 16(*a*) and 16(*c*). Comparison of the profiles 3 in

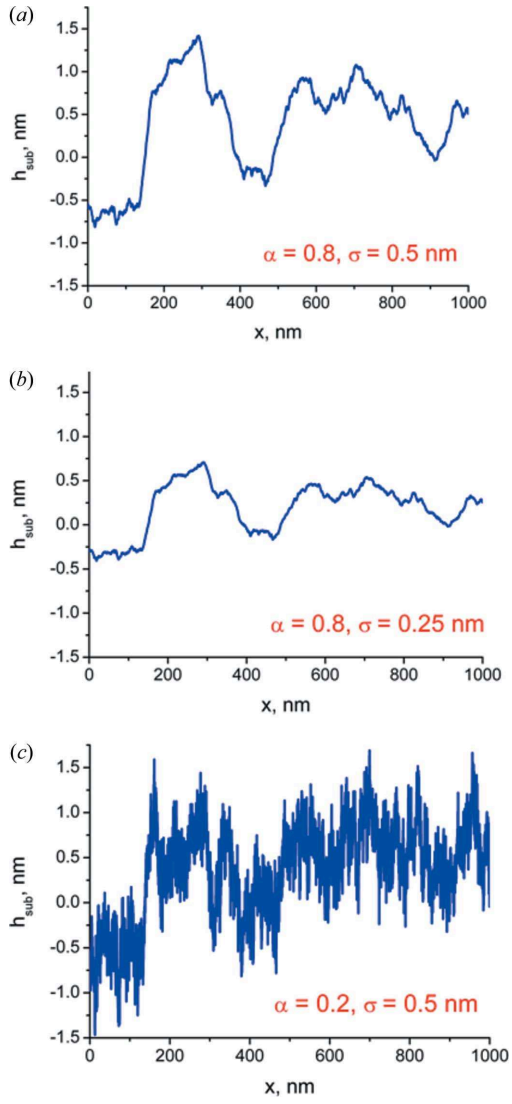

Figure 15
Three model rough surfaces with the correlation function (4) and the following roughness parameters: $\sigma = 0.5$ nm, $\alpha = 0.8$ (*a*), $\sigma = 0.25$ nm, $\alpha = 0.8$ (*b*) and $\sigma = 0.5$ nm, $\alpha = 0.2$ (*c*). The correlation length $\xi = 100$ nm is the same for all profiles. The roughness heights are distributed according to the normal law.

Figs. 16(*a*) and 16(*c*) shows that the spikes' width and the distance between two neighboring spikes decreases essentially with decreasing fractal parameter of the substrate, so that the profile in Fig. 16(*c*) correlates better with the experimental data. Notice that the fractal parameter of 0.2–0.3 and the correlation length of a fraction of micrometer are rather typical of the intrinsic roughness of several tens of nanometers thick films deposited by magnetron sputtering (see, for example, Filatova *et al.*, 2010; Peverini *et al.*, 2007). At the same time, a direct comparison of our calculations and experimental data is not totally correct because we use a simplified case of a 1+1-dimension surface when modeling the contamination layer growth. The use of a more realistic 1+2-dimensional surface model will be described in a future paper.

In summary, we have analyzed the growth of an adhesion layer on a rough substrate. The virgin surface roughness was

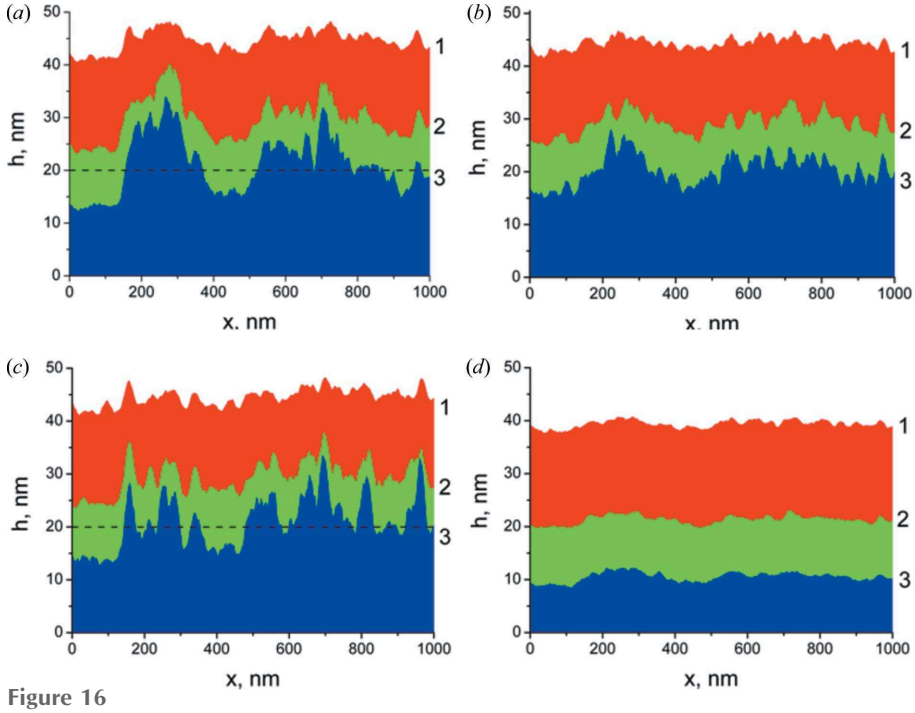

Figure 16
Profile of the contamination layer grown on a rough substrate. The graphs (*a*) and (*d*) correspond to the substrate (*a*) shown in Fig. 15, while graphs (*b*) and (*c*) to substrates (*b*) and (*c*), respectively. The polymerization parameter $\eta_0 = 0.25$ (*a*, *b*, *c*) or 0.05 (*d*). The ratio $P_{\rm des}/P_{\rm dif} = 1$, 3 and 9 for profiles 1, 2 and 3, respectively. The profiles were averaged over 10 nm intervals along the *x*-axis.

demonstrated to result in the growth of spikes from the beginning, if the radiation intensity is high enough. The growth occurs on substrate areas placed above the averaged surface. The statistical parameters of the spikes were shown to depend heavily on the roughness parameters of the virgin substrate.

6. Dependence of nano-dots growth on the grazing angle of an incident beam

Consider next the growth of spikes depending on the grazing angle of the incoming FEL beam. As was mentioned in the *Introduction*, an interesting observation is that, in contrast to mirror BL3M0, where the grazing angle was 3°, the spikes did not appear on the surface of mirror BL0M0 placed at 2° grazing angle with respect to the incident beam.

Surface profiles are shown in Fig. 17 after growth of a carboneous film of about 25 nm average thickness outside the spike area for different grazing angles of incident radiation varying from 1° to 10°. The feature on the virgin surface was the same as that in Fig. 13 with a maximal height of 1.5 nm. The radiation wavelength was set to 20 nm, and the parameter $\eta_0 = 0.75$ was fixed so that the probability of polymerization on a flat surface was changed from $P_0 = 1.56\%$ at $\theta = 1°$ to 75.0% at $\theta = 10°$, because of the quick increase in the field intensity on the surface with increasing grazing angle (see Fig. 18). The ratio $P_{\rm des}/P_{\rm dif} = 3/1$ was also fixed.

The spike of about 12 nm in height with respect to the average plane $h = \bar{h} = 25$ nm is clearly seen at the 3° grazing angle of the incident beam. However, if the grazing angle decreases to 2°, the spike is decreased to several nanometers and it is almost indistinguishable in the figure. This is because the variation in the field intensity (its derivative) near the surface is essentially less at the grazing angle $\theta = 2°$ compared with that at $\theta = 3°$ (see Fig. 18). Therefore, the effect of positive feedback on the spike growth is considerably reduced when the grazing angle is decreased from 3° to 2°. Further decrease in the grazing angle down to 1° results in the total disappearance of the spike.

If the grazing angle increases to 4° (Fig. 17*c*), the spike height achieves 15 nm with respect to the average surface plane. However, further increase in the grazing angle results in a decrease of the spike height and its disappearance at $\theta = 10°$. The probability of polymerization is extremely high in the last case and achieves 75% even on a flat surface, which is only slightly less compared with that at the top of the feature of 1.5 nm height. Hence, the surface growth occurs almost uniformly on average, because the probability of desorption is almost the same independent of the point on the surface, whether it is placed on the feature top or on the average surface.

Therefore, if the average thickness of the adhesion layer is fixed at 25 nm, the spikes' growth occurs at the limited, from above and below, interval of the grazing angle of incident radiation, namely 3–6° in the example considered.

7. Conclusions

Inspecting the state of the grazing-incidence mirror used at beamline BL3 of the XUV-FEL FLASH over three years, a completely unexpected physical phenomenon was detected: alot of nano-dots placed chaotically over the mirror surface were clearly observed (Fig. 2). The typical diameter d and height h of the nano-dots proved to lie in the intervals $d \simeq 40$–55 nm and $h \simeq 8$–13 nm. The space density of the dots is about 9.4 dots μm^{-2} and the distance l between neighboring dots is of the order of $l \simeq 100$–350 nm.

Polymerization of the hydrocarbon molecules contained in any vacuum under the action of photoelectrons allowed explanation of the occurrence and growth of nano-dots on the mirror surface, if the high intensity of the FEL beam, random fluctuations of the incoming flux of hydrocarbon molecules and the roughness of the virgin reflective surface were taken into account. The probability of polymerization is proportional to the radiation intensity. As the grazing angle of the incidence beam (wavelength $\lambda \simeq 45$ nm) is small ($\theta = 3°$), the field intensity on the surface is low (Fig. 5), while it is higher on

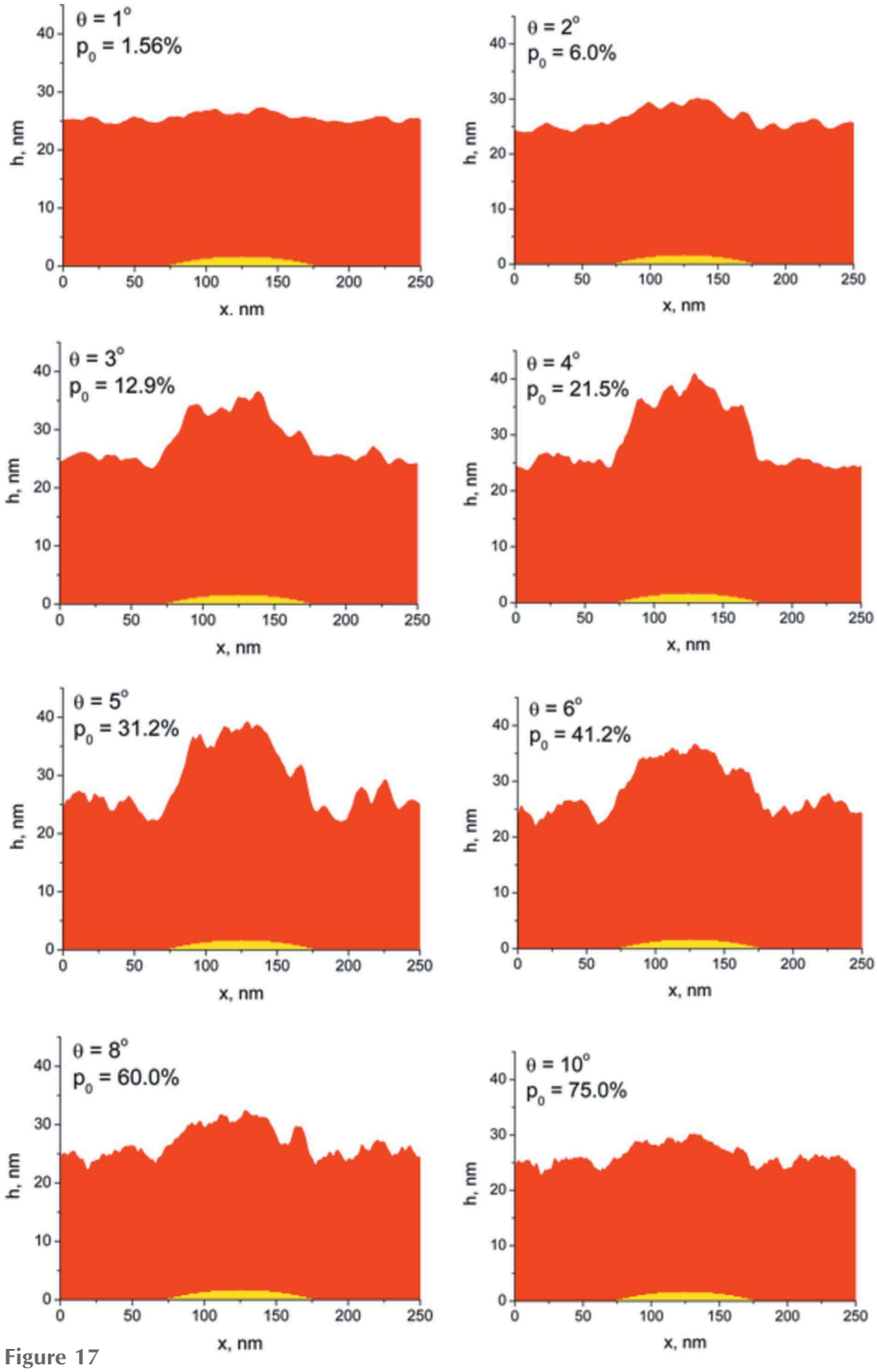

Figure 17
Growth of a carboneous layer on the substrate with the parabolic feature of 1.5 nm maximal height. The grazing angle of incident radiation ($\lambda = 20$ nm) is varied from $\theta = 1^\circ$ to 10°. Parameter $\eta_0 = 0.75$ such that the probability of polymerization on a flat surface is changed from $P_0 = 1.56\%$ at $\theta = 1^\circ$ to $P_0 = 75.0\%$ at $\theta = 10^\circ$. The values of θ and P_0 are shown in the figures. The ratio $P_{des}/P_{dif} = 3/1$ was fixed. The cubic size was $a = 0.25$ nm. The same sets of random numbers $\{j\}$ and $\{p\}$ were used when calculating different films. The profiles were averaged over 10 nm intervals along the X-axis.

the top of a feature placed on the surface. As a result, the growth rate of the polymerized film on the feature top increases compared with that on the underlying surface. Therefore, positive feedback arises: the higher the feature on the surface, the quicker its growth occurs, resulting in the appearance of dots.

The nano-dots were demonstrated to arise even on a perfectly smooth substrate (Fig. 10), if (*a*) the radiation flux density is high enough, (*b*) the probability of desorption of incoming hydrocarbon molecules is non-zero, and (*c*) the probability of the surface diffusion of the adsorbed molecules is not very high. The cause of the nano-dots occurrence in this case is stochastic fluctuations of the incoming molecule flux, and the nano-dots arise at large enough thickness (~120–150 nm) of the contamination layer (Fig. 10).

The growth of a contamination carboneous layer on a rough substrate was analyzed in more detail. The virgin surface roughness was demonstrated to result in nano-dots growth from the beginning, if the radiation intensity is high enough (Fig. 13). The growth occurs on substrate areas placed above the averaged surface, where the field intensity is higher. The presence of surface roughness of only several angstroms in height gives rise to nano-dots of about 10–15 nm height after growth of the contamination film of only 10–20 nm averaged thickness (Fig. 16).

The dependence of the nano-dots growth on the grazing angle of incoming radiation was analyzed. The growth of nano-dots was demonstrated to be clearly observed in a limited, from above and below, interval of the grazing angles (Fig. 17). On the one hand, the variation in the field intensity (its derivative) near the surface is enhanced with increasing grazing angle resulting in a strengthening of the positive feedback during spike growth. On the other hand, further increase in the grazing angle results in an essential increase in the polymerization probability tending to unity independently on a point where a molecule falls onto the surface, so that the surface growth occurs uniformly on average in this case. Decreasing the grazing angle from 3° to 2° was shown to essentially suppress the nano-dots growth in accordance with experimental observation.

In conclusion, our analysis was based on the study of two mirrors only. It is possible to imagine a number of factors other than the polymerization of incoming hydrocarbon molecules which cause the nano-dots growth. Nevertheless, we believe that our model is simple and motivated from the

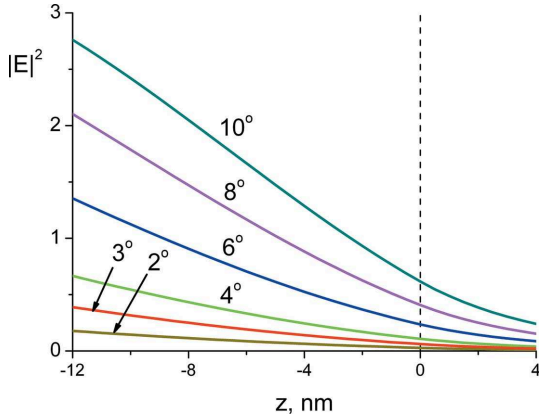

Figure 18
Field intensity (at λ = 20 nm) near an ideally smooth carbon surface placed at z = 0 for different grazing angles θ of the incident beam, the value of θ being indicated in the graph. The amplitude of the incident wave was set to unity for definiteness. The z-axis is directed into the substrate. The vertical dashed line shows the position of the reflecting surface.

physical point of view, and allowed us to explain (qualitatively, at least) all the observed phenomena.

Acknowledgements

Two of the authors (IVK and AVB) were supported by the Russian Ministry of Science and Education *via* the program 'Physics at the accelerators and reactors of the West Europe (excluding CERN)'.

References

Ackermann, W. *et al.* (2007). *Nat. Photon.* **1**, 336–342.
Anazawa, T., Nishiyama, Y., Oizumi, H., Suga, O. & Nishiyama, I. (2008). *Proceedings of the International Symposium on Extreme Ultraviolet Lithography* (Lake Tahoe, CA, USA, 28 September–1 October 2008, Vol. 3, p. 1611.
Asadchikov, V. E., Kozhevnikov, I. V., Krivonosov, Yu. S., Mercier, R., Metzger, T. H., Morawe, C. & Ziegler, E. (2004). *Nucl. Instrum. Methods Phys. Res. A*, **530**, 575–595.
Ayvazyan, V. *et al.* (2006). *Eur. Phys. J. D*, **37**, 297–303.
Barabási, A.-L. & Stanley, H. E. (1995). *Fractal Concepts in Surface Growth.* Cambridge University Press.
Boller, K., Haelbich, R.-P., Hogrefe, H., Jark, W. & Kunz, C. (1983). *Nucl. Instrum. Methods Phys. Res.* **208**, 273–279.
Chen, J., Louis, E., Lee, C. J., Wormeester, H., Kunze, R., Schmidt, H., Schneider, D., Moors, R., van Schaik, W., Lubomska, M. & Bijkerk, F. (2009). *Opt. Express*, **17**, 16969–16979.
Eggenstein, F., Senf, F., Zeschke, T. & Gudat, W. (2001). *Nucl. Instrum. Methods Phys. Res. A*, **467–468**, 325–328.
Family, F. (1986). *J. Phys. A*, **19**, L441–L446.
Family, F. & Vicsek, T. (1985). *J. Phys. A*, **18**, L75–L81.
Filatova, E. O., Kozhevnikov, I. V., Sokolov, A. A., Ubyivovk, E. V., Yulin, S., Gorgoi, M. & Schäfers, F. (2012*a*). *Sci. Technol. Adv. Mater.* **13**, 015001.
Filatova, E. O., Peverini, L., Ziegler, E., Kozhevnikov, I. V., Jonnard, P. & André, J.-M. (2010). *J. Phys. Condens. Matter*, **22**, 345003.
Filatova, E. O., Sokolov, A. A. & Kozhevnikov, I. V. (2012*b*). *High-k Gate Dielectrics for SMOS Technology*, ch. 7, edited by Gang He, pp. 225–271. Weinhem: Wiley-VCH Verlag.
Hau-Riege, S. P., London, R. A., Chapman, H. N. & Bergh, M. (2007). *Phys. Rev. E*, **76**, 046403.
Kozhevnikov, I. V., Filatova, E. O., Sokolov, A. A., Konashuk, A. S., Siewert, F., Störmer, M., Gaudin, J., Keitel, B., Samoylova, L. & Sinn, H. (2015). *J. Synchrotron Rad.* **22**, 348–353.
Kurt, R., van Beek, M., Crombeen, C., Zalm, P. & Tamminga, Y. (2002). *Proc. SPIE*, **4688**, 702–709.
Malinowski, M. E., Grunow, P. A., Steinhaus, C., Clift, W. M. & Klebanoff, L. E. (2001). *Proc. SPIE*, **4343**, 347–356.
Motai, K., Oizumi, H., Miyagaki, S., Nishiyama, I., Izumi, A., Ueno, T. & Namiki, A. (2008). *Thin Solid Films*, **516**, 839–843.
Naito, T., Tadano, M., Terunuma, N., Urakawa, J., Nakamura, E., Hasumoto, M., Sakai, H., Shibuya, T., Sakai, F., Ohgaki, H. & Sei, N. (2004). *Nucl. Instrum. Methods Phys. Res. A*, **527**, 624–631.
Oestreich, S., Klein, R., Scholze, F., Jonkers, J., Louis, E., Yakshin, A. E., Goerts, P. C., Ulm, G., Haidl, M. & Bijkerk, F. (2000). *Proc. SPIE*, **4146**, 64–71.
Peverini, L., Ziegler, E., Bigault, T. & Kozhevnikov, I. (2007). *Phys. Rev. B*, **76**, 045411.
Siewert, F., Buchheim, J., Zeschke, T., Störmer, M., Falkenberg, G. & Sankari, R. (2014). *J. Synchrotron Rad.* **21**, 968–975.
Störmer, M., Siewert, F. & Gaudin, J. (2011). *Proc. SPIE*, **8078**, 80780G.
Tiedtke, K., Azima, A., von Bargen, N., Bittner, L., Bonfigt, S., Düsterer, S., Faatz, B., Frühling, U., Gensch, M., Gerth, Ch., Guerassimova, N., Hahn, U., Hans, T., Hesse, M., Honkavaar, K., Jastrow, U., Juranic, P., Kapitzki, S., Keitel, B., Kracht, T., Kuhlmann, M., Li, W. B., Martins, M., Núñez, T., Plönjes, E., Redlin, H., Saldin, E. L., Schneidmiller, E. A., Schneider, J. R., Schreiber, S., Stojanovic, N., Tavella, F., Toleikis, S., Treusch, R., Weigelt, H., Wellhöfer, M., Wabnitz, H., Yurkov, M. V. & Feldhaus, J. (2009). *New J. Phys.* **11**, 023029.
Wyant, J. C. (2002). *Proc. SPIE*, **4737**, 98–107.